

Article

Synergistic Antifungal Efficiency of Biogenic Silver Nanoparticles with Itraconazole against Multidrug-Resistant Candidal Strains

Mohamed Taha Yassin *, Ashraf Abdel-Fattah Mostafa, Abdulaziz Abdulrahman Al-Askar and Fatimah O. Al-Otibi

Botany and Microbiology Department, College of Science, King Saud University, P.O. Box 2455, Riyadh 11451, Saudi Arabia; asali@ksu.edu.sa (A.A.-F.M.); aalaskara@ksu.edu.sa (A.A.A.-A.); falotibi@ksu.edu.sa (F.O.A.-O.)

* Correspondence: myassin2.c@ksu.edu.sa

Abstract: Fungal infections caused by multidrug-resistant strains are considered one of the leading causes of morbidity and mortality worldwide. Moreover, antifungal medications used in conventional antifungal treatment revealed poor therapeutic effectiveness and possible side effects such as hepatotoxicity, nephrotoxicity, and myelotoxicity. Therefore, the current study was developed to determine the antifungal effectiveness of green synthesized silver nanoparticles (AgNPs) and their synergistic efficiency with antifungal drugs against multidrug-resistant candidal strains. The AgNPs were greenly synthesized using the aqueous peel extract of *Punica granatum*. In addition, AgNPs were characterized using ultraviolet-visible spectrophotometry (UV/Vis), transmission electron microscopy (TEM), energy-dispersive X-ray spectroscopy (EDX), Fourier transform infrared spectroscopy (FT-IR), X-ray diffraction analysis (XRD), and zeta potential analysis. In this regard, UV-vis analysis indicated SPR of AgNPs at 396 nm, while the particle size distribution revealed that the average particle size was 18.567 ± 1.46 nm. The surface charge of AgNPs was found to be -15.6 mV, indicating their stability in aqueous solutions. The biofabricated AgNPs indicated antifungal activity against *Candida tropicalis*, *C. albicans*, and *C. glabrata* strains showing inhibitory zone diameters of 23.78 ± 0.63 , 21.38 ± 0.58 , and 16.53 ± 0.21 mm, respectively while their minimum inhibitory concentration (MIC) was found to be $2.5 \mu\text{g/mL}$ against *C. tropicalis* strain. AgNPs and itraconazole revealed the highest synergistic activity against the multidrug-resistant strain, *C. glabrata*, recording a synergism percentage of 74.32%. In conclusion, the biogenic AgNPs in combination with itraconazole drug exhibited potential synergistic activity against different candidal strains indicating their potential usage in the bioformulation of highly effective antifungal agents.

Keywords: resistance; green synthesis; silver nanoparticles; antifungal activity; synergism



Citation: Yassin, M.T.; Mostafa, A.A.-F.; Al-Askar, A.A.; Al-Otibi, F.O. Synergistic Antifungal Efficiency of Biogenic Silver Nanoparticles with Itraconazole against Multidrug-Resistant Candidal Strains. *Crystals* **2022**, *12*, 816. <https://doi.org/10.3390/cryst12060816>

Academic Editor: Witold Łojkowski

Received: 10 May 2022

Accepted: 6 June 2022

Published: 8 June 2022

Publisher's Note: MDPI stays neutral with regard to jurisdictional claims in published maps and institutional affiliations.



Copyright: © 2022 by the authors. Licensee MDPI, Basel, Switzerland. This article is an open access article distributed under the terms and conditions of the Creative Commons Attribution (CC BY) license (<https://creativecommons.org/licenses/by/4.0/>).

1. Introduction

Fungal infections are a major public health concern that cause a high rate of morbidity and mortality worldwide, accounting for approximately 1.7 million deaths annually [1,2]. In this regard, high doses of antifungal agents are required for the treatment of candidal infections caused by multidrug-resistant candidal strains, which result in severe toxicity and unfavorable side effects [3]. The main classes of antifungal agents are reported to be polyenes, allylamines, flucytosine, azole, and echinocandins [4]. In this regard, antifungal agents target cell wall components of fungal cells [5]. Azoles are usually used as the first line in the treatment of fungal infections [6]. The mechanism of action of azole antifungal agents is based on the inhibition of the lanosterol 14- α -demethylase (Erg11p) enzyme, which is coded by the ERG11 gene and responsible for ergosterol biosynthesis [7]. Inhibition of Erg11p enzyme biosynthesis results in disrupting cell membrane integrity and consequently inhibiting fungal growth [8]. Azole antifungal resistance is mediated by the alteration of

the ERG11 gene and mutations of the ergosterol biosynthesis pathway [9]. Moreover, antifungal resistance also occurs due to overexpression of the ERG11 gene, which results in increasing ergosterol biosynthesis and disrupting the efficiency of antifungal drugs [10]. Furthermore, antifungal resistance is also promoted by the overexpression or upregulation of multidrug transporters, enhancing drug efflux and inhibiting azole accumulation [11]. *Candida glabrata* is a multidrug-resistant fungal pathogen which is characterized by its high resistance to fluconazole antifungal agent [12]. The high incidence of multidrug-resistant candidal species of bloodstream infections represents a global concern due to the high mortality rate associated with these infections [13]. Accordingly, the high emergence of antifungal resistance necessitates the formulation of novel biomaterials to improve the therapeutic outcomes [14].

Metallic nanoparticles were reported to be promising alternatives to conventional antimicrobial agents that can defeat common microbial resistant mechanisms, including the modification of the target site, increased drug efflux through overexpression of efflux pumps, enzyme inactivation, and decreased cell membrane permeability [15]. Metallic nanoparticles reveal various advantages in this context, including tiny particle size (1–100 nm), minimal cytotoxicity, excellent chemical stability, and promising antimycotic efficacy [16]. Silver nanoparticles are reported to have a high potential for inhibiting mycotic growth and preventing microbial resistance [17]. Silver nanoparticles are easily synthesized and have unique physical and chemical characteristics [18]. Reportedly, silver nanomaterials exhibit promising antimicrobial effectiveness against fluconazole-resistant *C. tropicalis* [19].

Different approaches have been achieved to fabricate silver nanoparticles, including chemical, physical, and biological methods [20]. The chemical method of nanomaterial synthesis yields high productivity; however, when employing a chemical approach to formulate AgNPs, hazardous reducing and capping chemicals are required for synthesis, causing the adsorption of toxic chemicals on nanoparticles, resulting in issues during application [21]. For green biosynthesis of nanomaterials utilizing plant extracts, on the other hand, less toxic stabilizing and reducing agents are used [22]. Furthermore, the reaction mechanism for the synthesis of biogenic silver nanomaterials utilizing plant extracts could be conducted in natural settings without the need for harsh or rigorous reaction conditions [23]. Another advantage of plant extract-mediated green produced nanomaterials is the decreased cytotoxicity of these green nanoparticles [24].

Antifungal resistance poses a significant clinical issue to clinicians who treat invasive mycotic infections owing to the defined number of systemically applicable antimycotic drugs [25]. In addition, current antifungal drugs may be limited by drug–drug interactions, detrimental side effects, and high toxicities, which hinder their continued usage for long term treatment [26]. Green synthesized nanoparticles, which were previously reported to have various advantages such as tiny size, biocompatibility, large surface area to volume ratio, and low toxicity, are used for circumventing the above-mentioned restrictions [27]. A previous report indicated the synergistic antifungal activity of chemically synthesized AgNPs with either nystatin or chlorhexidine digluconate against *C. glabrata* and *C. albicans* strains [28]. Another study indicated that the synergistic action of AgNPs and fluconazole antifungal drugs could be a potential way to treat fluconazole-resistant fungal infections [29]. Furthermore, poly(methacrylic acid)-AgNPs possessed synergistic action with fluconazole antifungal drug against fluconazole-resistant *C. albicans* strains through suppression of germ tube formation [30]. Recently, several reports reported the high incidence of candidal resistance to conventional antifungal drugs [31–34], indicating the poor therapeutic outcomes of these antifungal agents. As a result, new antifungal formulations are needed to enhance the antifungal effectiveness of conventional antifungal agents so that the synergistic efficiency of biogenic AgNPs with five common antifungal agents such as clotrimazole, fluconazole, itraconazole, nystatin, and terbinafine can be evaluated. Furthermore, few studies were performed regarding the synergistic efficiency of the green synthesized AgNPs with the mentioned antifungal agents. Therefore, the

objective of the present study is to detect the antimycotic efficiency of AgNPs greenly synthesized using aqueous peel extract of *P. granatum* and to determine their synergistic efficiency with commonly used antifungal agents to enhance the therapeutic outcomes of these drugs.

2. Materials and Methods

2.1. Preparation of Pomegranate Extract

Punica granatum fruits were acquired in Riyadh, Saudi Arabia, at a local market. The identification of plant material was confirmed by the herbarium of the Botany and Microbiology Department, College of Science, King Saud University, and the plant materials were deposited with voucher number (KSU_14702). The pomegranate peels were rinsed twice with tap water before being scrubbed once more with distilled water. After drying, the peels were pulverized into a homogeneous powder using a mechanical mortar. In total, 50 g of powdered peels were placed in 500 mL flasks with 200 mL of deionized water and cooked for 30 min on a hot plate at 50 °C. The extracts were filtered using Whatman filter paper grade 1 after being incubated at 25 °C for 24 h over a magnetic stirrer. The peel extracts were kept in the refrigerator at 4 °C for further use [35].

2.2. Green Synthesis of Silver Nanoparticles

Silver nitrate (AgNO_3) salt was supplied by Sigma-Aldrich, MO, USA. Green synthesis of silver nanoparticles was achieved by adding 10 mL of the aqueous peel extract of *P. granatum* to 90 mL of AgNO_3 solution (1 mM). The reaction mixture was incubated in dark conditions over a shaking incubator at 24 °C. The change of AgNO_3 solution from colorless to dark brown color primarily indicated AgNPs formation. The green biosynthesized AgNPs were harvested by centrifuging the reduced reaction mixture for 10 min at 10,000 rpm. After discarding the supernatant, the harvested AgNPs were washed three times using distilled H_2O and finally dried at 80 °C in an oven. The dried AgNPs were used for further analysis and characterization [36].

2.3. Characterization of the Biosynthesized AgNPs

The biosynthesized AgNPs were characterized for the detection of their physicochemical properties. UV-Vis spectral analysis of biogenic AgNPs synthesized using aqueous peel extract of *P. granatum* was conducted using a UV-Vis spectrophotometer (UV-1601, Shimadzu, Kyoto, Japan) [37]. A transmission electron microscope (JEOL, JEM1011, Tokyo, Japan) was used to detect the nanoparticles' shape and their particle size distribution [38]. Sonication of AgNPs was performed for 5 min prior to analysis, and a drop of properly diluted sample was placed onto a carbon-coated copper grid. Fourier transform infrared (FTIR) spectral analysis was conducted to detect different functional groups in the aqueous peel extract of *P. granatum* peels, acting as reducing and capping agents of AgNPs. The elemental mapping of AgNPs was investigated using a Scanning Electron Microscope (SEM) equipped with an Energy Dispersive X-ray (EDX) analyzer (JEOL, JSM-6380 LA, Tokyo, Japan). X-ray powder diffraction (XRD) analysis of AgNPs was achieved using a Shimadzu XRD model 6000 diffractometer (Japan) equipped with a graphite monochromator to detect crystallographic characteristics of AgNPs [39]. Zeta potential analysis of AgNPs was characterized using a Zeta sizer instrument (Malvern Instruments Ltd.; zs90, Worcestershire, UK) to investigate the surface charge of the biogenic AgNPs based on photon correlation spectroscopy.

2.4. Screening of Anticandidal Efficiency of Biogenic AgNPs

Three candidal strains namely, *C. albicans* (ATCC 18804), *C. tropicalis* (ATCC 13803), and *C. glabrata* (ATCC 15545), were obtained from the American Type Culture Collection. The anticandidal activity of biogenic AgNPs synthesized using aqueous peel extract of *P. granatum* against the tested Candida strains was investigated using the standard procedure for disk diffusion testing no M44-A [40]. Firstly, the candidal suspension

was prepared by gathering the fungal growth of 24 h old candidal colonies using a sterile loop and disseminating it into a sterile saline solution (0.85%). The turbidity of the fungal suspension was adjusted using 0.5 McFarland standards which correspond to 10^6 CFU/mL. The sterile Mueller Hinton agar (MHA) medium (Oxoid, Ltd., Hampshire, UK) supplemented with 0.5 $\mu\text{g}/\text{mL}$ of methylene blue and 2% glucose was dispensed into sterile Petri dishes, and then the plates were seeded with 0.2 mL of the prepared fungal suspension. The dried AgNPs were disbanded in methanol solvent, and then 50 and 100 μg of the dissolved AgNPs were impregnated into sterile filter paper disks 8 mm in diameter. Positive controls were filter paper disks loaded with terbinafine antifungal agent at a concentration of 30 $\mu\text{g}/\text{disk}$, while filter paper disks impregnated with methanol solvent only were used as negative controls. The AgNPs, positive and negative control disks, were placed over the MHA plates, and the Petri dishes were then maintained in the refrigerator for 2 h at 4 $^{\circ}\text{C}$ to allow AgNPs diffusion. The plates were incubated at 35 ± 2 $^{\circ}\text{C}$ for 48 hr, and the clear zones were measured with a Vernier caliper afterwards. Moreover, the aqueous pomegranate peel extract (APPE) was investigated for the antifungal activity against the tested strains to compare the antimicrobial efficiency with that of biogenic AgNPs. In this regard, another group of filter paper disks (8 mm in diameter) were impregnated with 100 $\mu\text{g}/\text{disk}$ of the aqueous pomegranate peel extract and placed over sterile MHA plates previously seeded with the concerned candidal suspensions. Similarly, filter paper disks loaded with sterile distilled water were used as negative controls, while another group of filter paper disks loaded with terbinafine antifungal concentration (30 $\mu\text{g}/\text{disk}$) were used as positive controls. After a 24 h incubation period, the plates were investigated for antimicrobial activity. Minimum inhibitory concentration (MIC) was measured using a broth microdilution assay as stated in CLSI document M27-Ed4 to determine the least concentration of AgNPs showing antifungal efficiency [41]. To determine MFC values, 10 μL of MIC wells with no obvious candidal growth were streaked over MHA plates, which were then incubated at 35 ± 2 $^{\circ}\text{C}$ for 48 h before being examined for candidal growth. MFC was found to be the lowest concentration of AgNPs that showed no candidal growth [42].

2.5. Determination of Synergistic Activity of Biogenic AgNPs with Common Antifungal Drugs

The synergistic effectiveness of AgNPs in combination with regularly used antifungal drugs against the concerned candidal strains was evaluated using the disk diffusion method [43,44]. Antifungal standards of itraconazole, fluconazole, nystatin, terbinafine, and clotrimazole were purchased from Sigma-Aldrich, MO, USA. Sterile filter paper disks (8 mm in diameter) were loaded with 10 μg , 25 μg , 20 μg , 30 μg , and 10 μg of itraconazole, fluconazole, nystatin, terbinafine, and clotrimazole as antifungal agents, respectively, while, another group of filter paper disks was impregnated with the same concentration of antifungal drugs plus the MIC concentration of AgNPs. In addition, filter paper disks impregnated with methanol solvent only were used as negative controls. Finally, disks loaded with AgNPs (2.5 $\mu\text{g}/\text{disk}$) were prepared to compare the antimicrobial efficiency with the other groups. Seeded MHA plates were prepared as mentioned above, and then the loaded filter paper disks were placed over the seeded plates. Consequently, each plate had four filter paper disks impregnated with the following: biogenic AgNPs (MIC concentration), antifungal drugs, AgNPs in combination with antifungal agents, and negative control disks. The plates were incubated at 25 $^{\circ}\text{C}$ for 24 hr after being preserved for 2 hr in a refrigerator to allow AgNPs diffusion. Finally, the plates were checked for inhibition zone formation, and the zone diameters were recorded using a Vernier caliper. The synergistic efficiency was measured by the equation $\frac{B-A}{A} \times 100$, where A and B are the inhibition zone diameters for antifungal and antifungal + silver nanoparticles, respectively [45,46].

2.6. Statistical Analysis

Statistical analysis of antifungal activity data was conducted using GraphPad Prism 5.0 (GraphPad Software, Inc., La Jolla, CA, USA) with a one-way analysis of variance and Tukey's test. The data were tabulated as the mean of triplicates \pm standard error.

3. Results and Discussion

3.1. UV-Vis Spectral Analysis

Figure 1A show the colorless AgNO_3 solution which was reduced by the aqueous extract of *Punica granatum* peels (Figure 1B). The observed change in color of AgNO_3 solution from colorless to dark brown after the addition of pomegranate peel extract was a preliminary sign of AgNPs formation, as seen in Figure 1C. The formation of AgNPs was affirmed using UV-Vis analysis of the reduced silver nitrate solution. In this setting, broad peak formation was detected at a wavelength of 396 nm, which indicated surface plasmon resonance (SPR) of the biosynthesized AgNPs in the reaction mixture, as seen in Figure 2. Our findings matched those of a previous study that found an absorption band at 396 nm, confirming the biosynthesis of AgNPs utilizing grape juice extracts [47]. Nanoparticles' size, aggregation, and the presence of stabilizing agents in the reaction medium were all found to influence the intensity of SPR production [48].

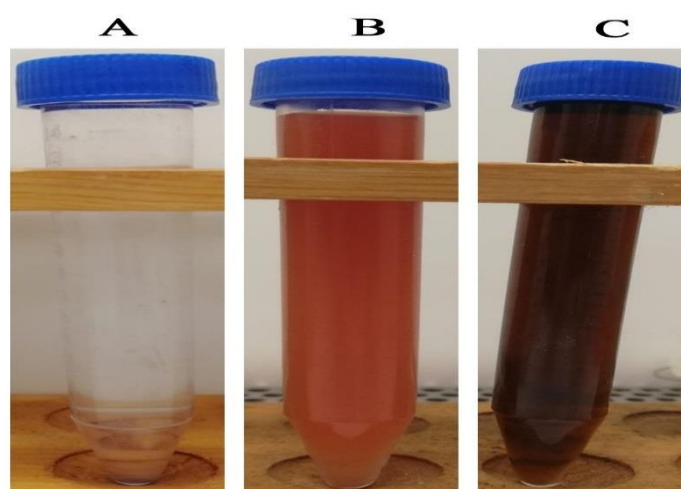


Figure 1. Change of color silver nitrate solution after addition of pomegranate peel extract confirming the biosynthesis of silver nanoparticles. ((A) colorless silver nitrate solution; (B) pomegranate peel aqueous extract; (C) the biosynthesized AgNPs).

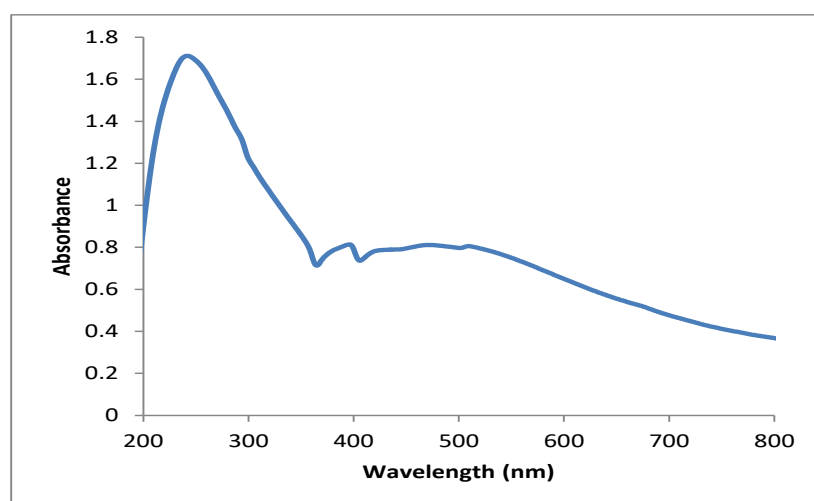


Figure 2. UV-vis spectrum of the biogenic AgNPs synthesized utilizing pomegranate peel extract.

3.2. TEM Characterization of the Biogenic Silver Nanoparticles

Transmission electron microscopy examination is the most accurate approach for determining the nanoparticle shape and average particle size of the bio-fabricated AgNPs [49]. A TEM micrograph of the bio-formulated AgNPs revealed the biosynthesis of well dispersed

and spherical silver nanoparticles, as seen in Figure 3. The biogenic AgNPs were found to be in the range of 5 to 100 nm, as clearly shown in TEM micrographs. A particle size distribution graph was constructed using TEM micrographs and indicated the formation of AgNPs with an average size of 18.425 ± 1.12 nm, as seen in Figure 4. Furthermore, due to the small estimated particle size, the particle size distribution verified the excellent efficiency of AgNPs synthesis utilizing *P. granatum* aqueous peel extract. Our results were in accordance with that of a previous study which demonstrated the bioformulation of AgNPs of average particle size of 18 nm using aqueous *Naringi crenulate* leaf extract [50]. However, the estimated average particle size was smaller than that of a recent study, which found that *Crataegus microphylla* extract facilitated bioformulation of AgNPs with an average size of 40 nm, as demonstrated by TEM micrographs [51].

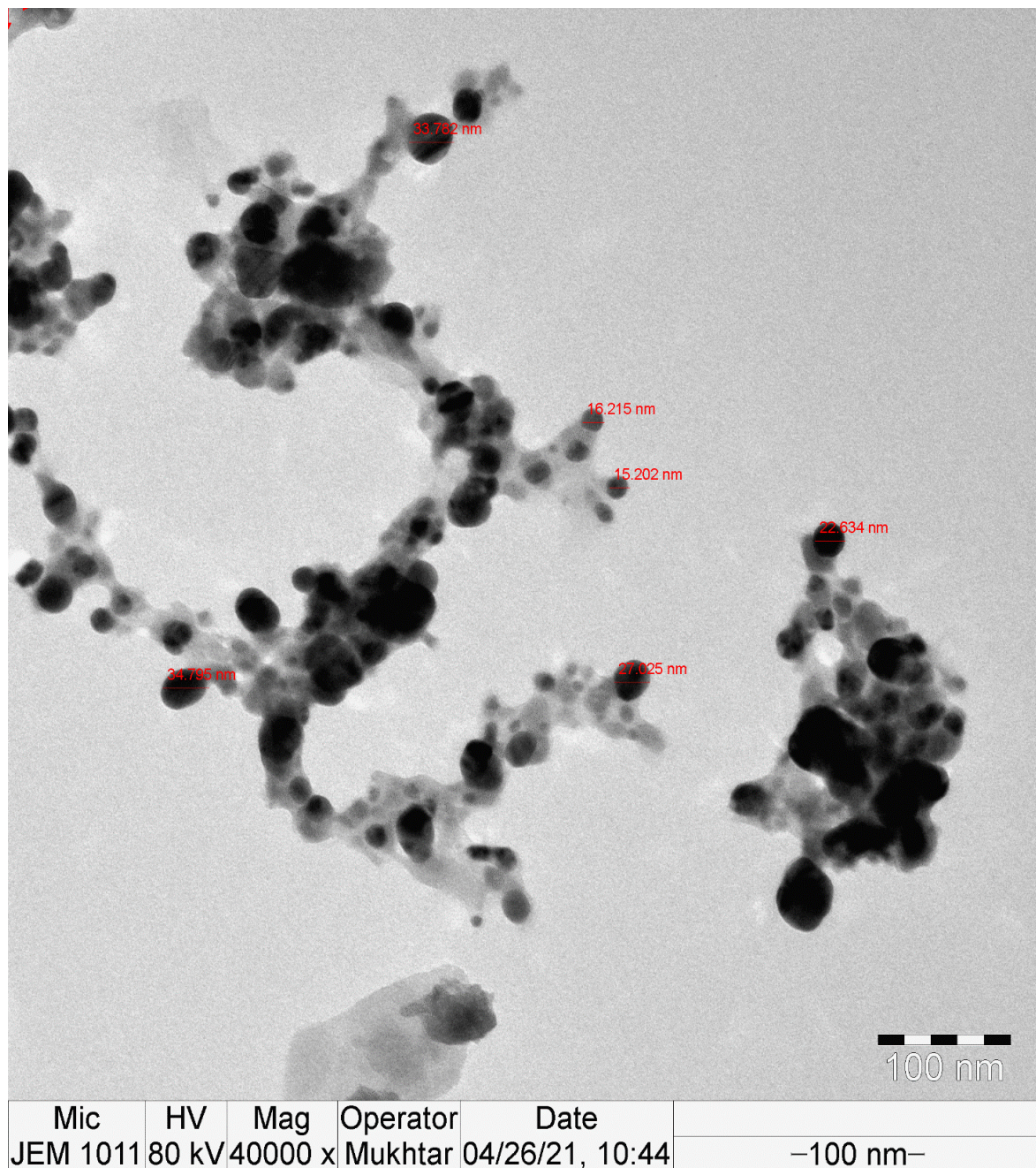


Figure 3. TEM micrograph of the bioinspired silver nanoparticles synthesized using aqueous peel extract of *Punica granatum*.

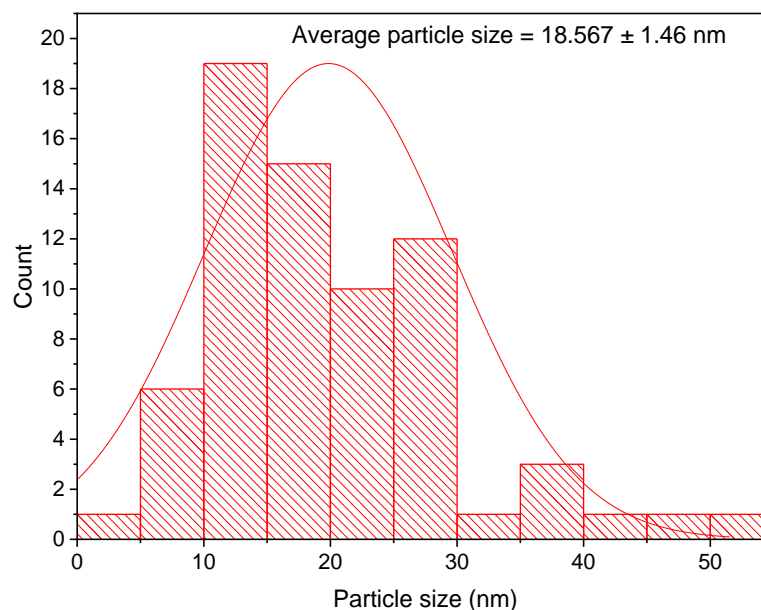


Figure 4. Particle size distribution histogram of AgNPs synthesized utilizing *Punica granatum* aqueous peel extract.

3.3. FTIR Analysis of the Biogenic Silver Nanoparticles

The biogenic AgNPs were analyzed using FTIR to identify the different functional groups that were responsible for the reduction and stability of the produced nanomaterials. As shown in Figure 5, the FTIR spectrum showed the presence of many absorption peaks, each of which was ascribed to a different functional group. The vibrational frequencies of the biogenic AgNPs were found at 3434.45, 1695.50, 1626.46, 1448.63, 1339.07, 1112.58, 1056.97, 757.10, and 579.43 cm^{-1} , corresponding to different functional groups of the biogenic AgNPs. The broad absorption peak at 3434.45 cm^{-1} was assigned for O-H stretching vibration, which indicated the presence of alcoholic and phenolic groups. The hydroxyl groups of phenolic and alcoholic groups were attached to the surface of silver nanoparticles, acting as a capping agent to prevent nanoparticle agglomeration and enhance the stability of the medium [52]. Furthermore, the absorption bands at 1695.50 and 1626.46 cm^{-1} suggested the presence of C=O and C=C stretching vibrations, respectively, corresponding to conjugated alkenes and aldehydes, as seen in Table 1. Moreover, the bands at 1339.07, 1112.58 and 1056.97 cm^{-1} were assigned for the presence of proteins, while the absorption bands at 1448.63 and 757.10 cm^{-1} indicated the presence of C-H bending, which were assignable for the presence of aromatic groups. In this context, the identified amino functional groups of proteins were previously found to act as stabilizing agents for silver nanoparticles and prevent their agglomeration [53].

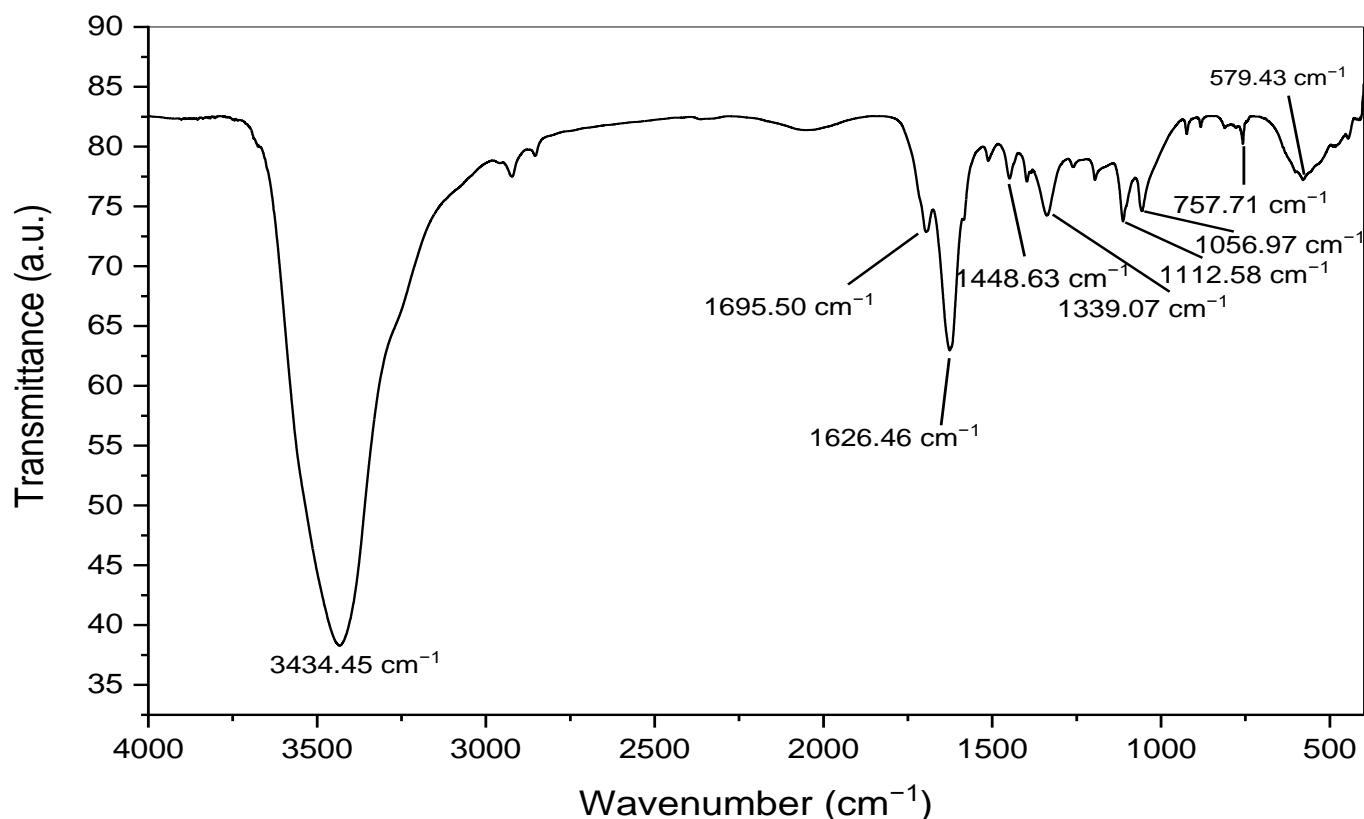


Figure 5. FTIR spectrum of the biogenic silver nanoparticles synthesized utilizing *Punica granatum* peel extract.

Table 1. Functional groups of silver nanoparticles fabricated using aqueous peel extract of *Punica granatum*.

No.	Absorption Peak (cm ⁻¹)	Appearance	Functional Groups	Molecular Motion
1	3434.45	Strong, broad	Alcohols and phenols	O-H stretching
2	1695.50	Medium	Conjugated aldehyde	C=O stretching
3	1626.46	Medium	Conjugated alkene	C=C stretching
4	1448.63	Medium	Aromatic group	C-H bending
5	1339.07	Medium	Amine	C-N stretching
6	1112.58	Medium	Amine	C-N stretching
7	1056.97	Medium	Amine	C-N stretching
8	757.71	Weak	Aromatic group	C-H bending
9	579.43	Strong, broad	Halo compound	C-Br stretching

3.4. Edx Analysis of the Biosynthesized AgNPs

The elemental analysis of the biogenic AgNPs was performed utilizing the Energy-dispersive X-ray spectroscopy (Edx) technique. Edx analysis revealed that silver was the main component, recording 60.92%, followed by carbon (16.91%), oxygen (15.19%), silicon (3.83%), and chloride (2.43%). The elemental mapping showed robust signals at 3.0 keV resulting from silver atoms confirming the successful formation of silver nanoparticles as seen in Figure 6, and our findings were in accordance with that of previous reports [54,55]. The silver percentage was significantly higher than that found in a previous study, which found that *Gleichenia Pectinata* facilitated the green synthesis of silver nanoparticles with an elemental silver percentage of 16% based on Edx results [56].

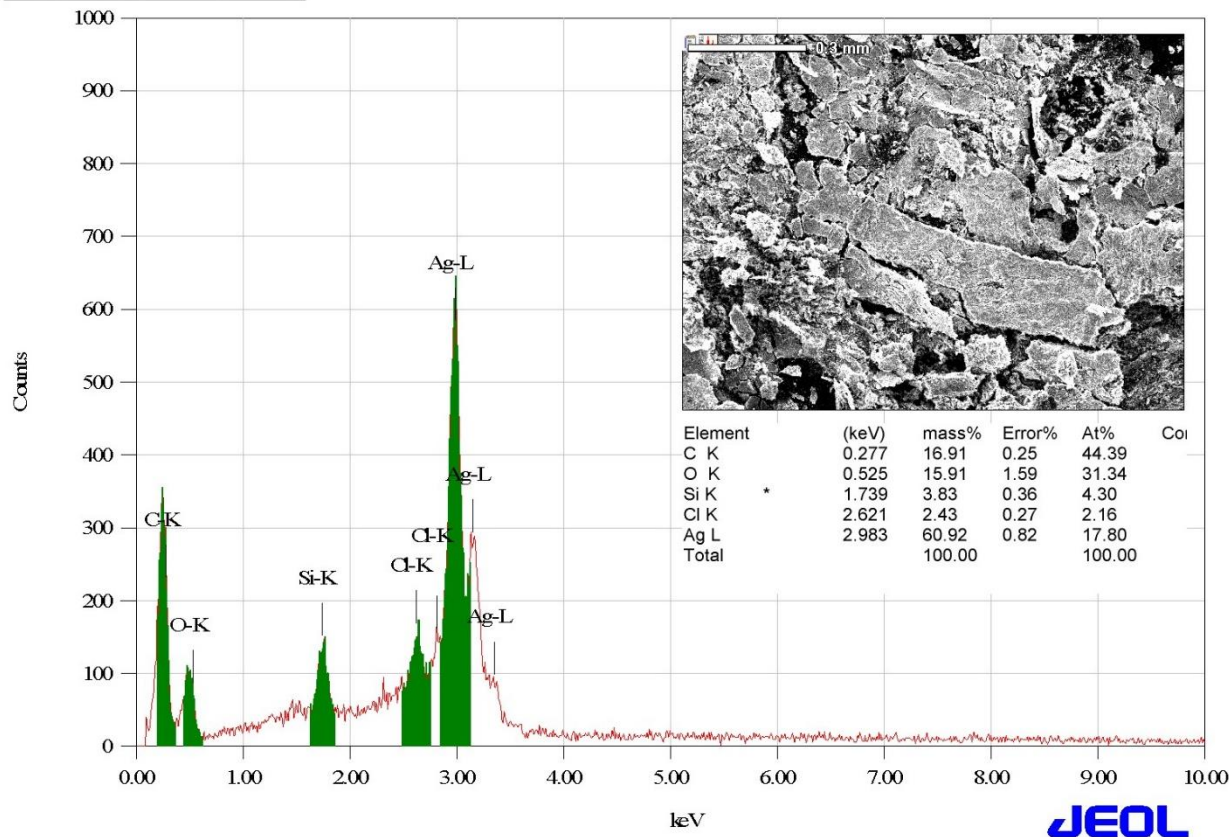
JED-2200 Series

Figure 6. Edx spectrum of the biogenic silver nanoparticle synthesized using aqueous peel extract of *Punica granatum*.

3.5. XRD Analysis of the Biogenic Silver Nanoparticles

XRD analysis was carried out in order to determine the crystalline nature of the synthesized AgNPs. The crystalline analysis of the biogenic AgNPs indicated the formation of five diffraction peaks at 2θ values of 28.0759, 38.1934, 44.2502, 65.3250, and 77.5620, as seen in Figure 7. The formation of the crystalline structure of face-centered cubic was confirmed by the Bragg reflections at 2θ degrees of 38.1934, 44.2502, 65.3250, and 77.5620, corresponding to the planes (111), (200), (220), and (311) of silver crystals, respectively, as stated by the Joint Committee on Powder Diffraction Standards (JCPDS), file No. 04-0783 [57]. The unidentified peak at a 2θ value of 28.0759 may be attributed to the formation of silver oxides, as reported by a previous study [58].

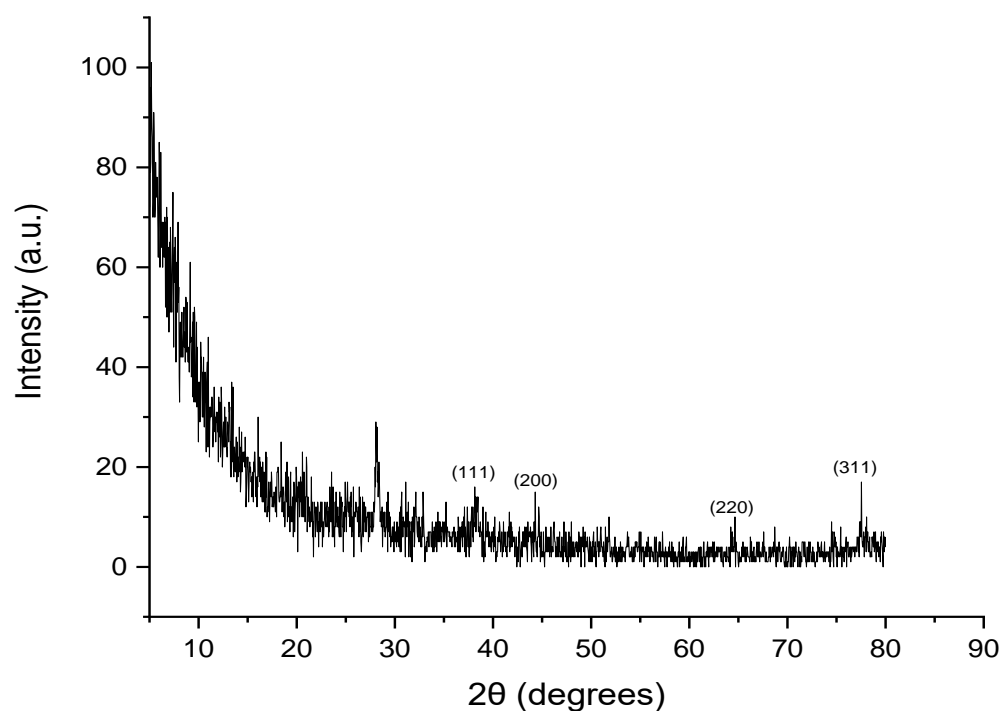


Figure 7. XRD spectrum of silver nanoparticles biosynthesized using aqueous peel extract of *Punica granatum*.

3.6. Zeta Potential Analysis of the Biosynthesized Silver Nanoparticles

Dynamic light scattering showed that the average hydrodynamic diameter of the biosynthesized AgNPs was 49.95 nm with a polydispersity index of 0.640 (Figure 8). The estimated average size of AgNPs in an aqueous solution detected by dynamic light scattering was higher than that detected by TEM analysis and could be assigned to the accumulation of extra hydrate layers on the AgNPs' surface. Zeta potential analysis is an important technique for the determination of the surface charge of silver nanoparticles which is a crucial factor for their stability in an aqueous medium [59]. Accordingly, the negative charge on the surface of the biosynthesized AgNPs revealed the electrostatic repulsion between them, which plays an important role in stability [60,61]. The estimated zeta potential values of the bio-inspired AgNPs were found to be -15.6 mV, as seen in Figure 9. Taken together, the negative charge of the biogenic AgNPs could be assigned to the capping action of the biomolecules of the pomegranate peel extract.

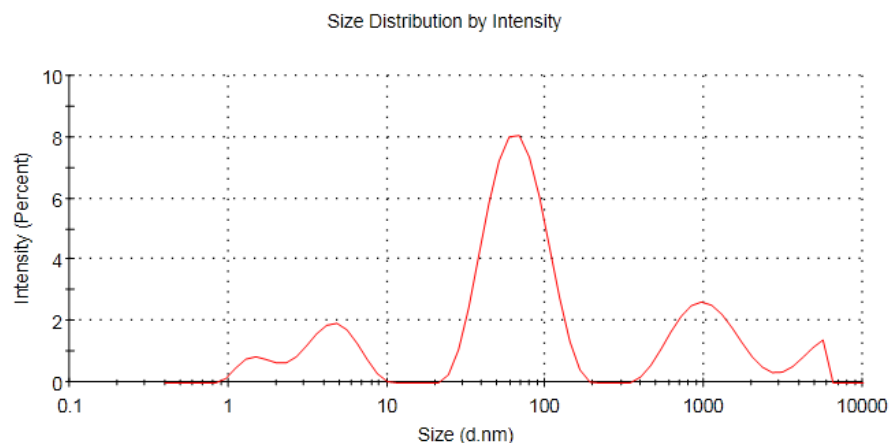


Figure 8. Dynamic light scattering of the biogenic AgNPs synthesized using aqueous peel extract of *Punica granatum*.

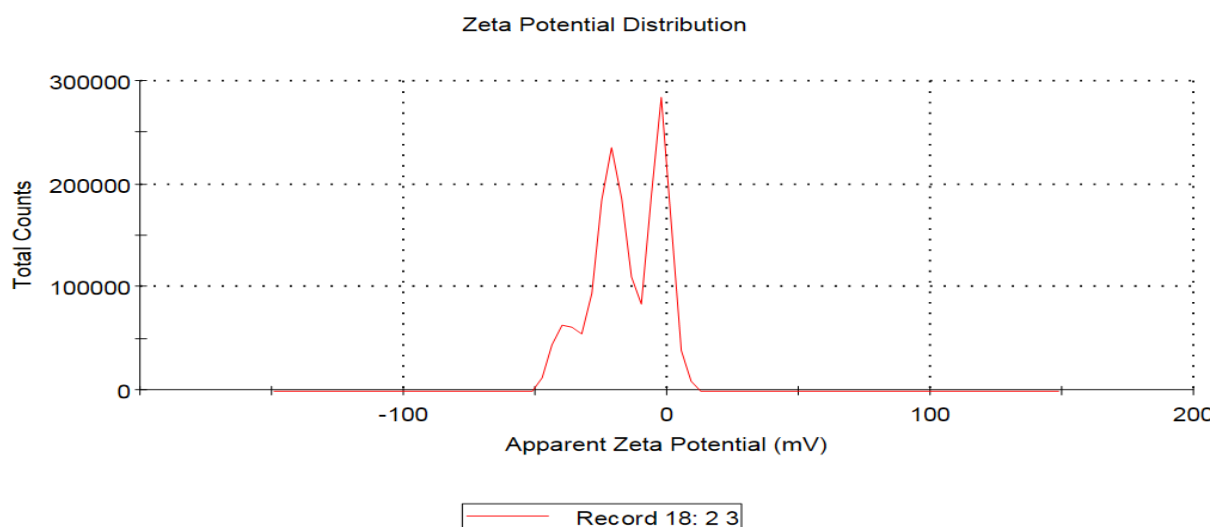


Figure 9. Zeta potential analysis of the biosynthesized AgNPs formulated using pomegranate peel extract.

3.7. Screening of Anticandidal Activity of the Biogenic AgNPs

The biogenic AgNPs were screened for their anticandidal activity against *C. albicans*, *C. glabrata*, and *C. tropicalis*. The disc diffusion method was utilized to detect the susceptibility of the concerned candidal strains to different concentrations of AgNPs. In this regard, *C. tropicalis* was the most sensitive strain to the biosynthesized AgNPs formulated using aqueous peel extract of *Punica granatum* at 50 and 100 $\mu\text{g}/\text{disc}$, with inhibitory zone diameters of 20.67 ± 0.41 and 23.78 ± 0.63 mm, respectively, as seen in Table 2. Furthermore, the biogenic AgNPs of concentrations 50 and 100 $\mu\text{g}/\text{disc}$ exhibited anticandidal efficiency against the *C. glabrata* strain with inhibitory zones of 13.89 ± 0.45 and 16.53 ± 0.21 mm, respectively, which were significantly higher than that of the control ($p \leq 0.05$). In contrast, a previous study revealed that the *C. glabrata* strain was the most sensitive to silver nanoparticles greenly synthesized using curcumin, while the *C. tropicalis* strain revealed the lowest sensitivity, with inhibitory zone diameters of 22.2 ± 0.8 and 16.4 ± 0.7 mm, respectively [19]. Moreover, the biogenic AgNPs exhibited antifungal efficiency against *C. albicans*, recording zone diameters of 18.13 ± 0.46 and 21.38 ± 0.58 mm, respectively. Our results were consistent with that of a prior study that reported the antifungal efficiency of AgNPs (60 μL) formulated using aqueous leaf extract of *Alhagi graecorum*, recording suppressive zones of 14 and 21 mm against *C. albicans* and *C. tropicalis* strains, respectively [62]. In contrast, the aqueous extract of pomegranate peel exhibited no antifungal efficiency against the concerned strains. This finding was in accordance with that of Endo et al., 2010 who reported that the crude extract of pomegranate peel showed no antifungal efficiency against the *C. albicans* strain [63].

Table 2. Screening of antimicrobial efficiency of *P. granatum* silver nanoparticles against the concerned candidal strains.

Concentration ($\mu\text{g}/\text{Disk}$)	Inhibition Zone Diameter (mm)		
	<i>C. albicans</i>	<i>C. glabrata</i>	<i>C. tropicalis</i>
AgNPs (50 $\mu\text{g}/\text{disk}$)	18.13 ± 0.46	13.89 ± 0.45	20.67 ± 0.41
AgNPs (100 $\mu\text{g}/\text{disk}$)	21.38 ± 0.58	16.53 ± 0.21	23.78 ± 0.63
APPE extract (100 $\mu\text{g}/\text{disk}$)	0.00 ± 0.00	0.00 ± 0.00	0.00 ± 0.00
Terbinafine (50 $\mu\text{g}/\text{disk}$)	28.53 ± 0.23	8.91 ± 0.35	34.63 ± 0.46
(-ve) control	0.00 ± 0.00	0.00 ± 0.00	0.00 ± 0.00

APPE: Aqueous pomegranate peel extract.

The minimum inhibitory concentration of the biogenic AgNPs was investigated against *C. tropicalis*, which demonstrated the highest susceptibility to the biogenic AgNPs (Figure 8). The MIC of biogenic AgNPs against the *C. tropicalis* strain was 2.5 µg/mL, while the MFC value was found to be 5 µg/mL. Our results were consistent with that of a previous study that revealed that the green synthesized AgNPs synthesized using *Parrotiopsis jacquemontiana* (Decne) Rehder leaf extract revealed anti-*candida* activity recording MIC and MFC values of 5 and 10 µg/mL, respectively [64]. Furthermore, a previous report demonstrated that silver nanoparticles synthesized using aqueous extract of aerial parts of *Pulicaria vulgaris* revealed antimycotic efficiency against *C. glabrata* and *C. albicans*, recording MIC values ranging from 40 to 60 µg/mL [65]. Taken together, the low MIC value of the biosynthesized AgNPs attained in our current study indicated their high efficiency as antifungal agents against the etiological agents of candidiasis.

3.8. Synergistic Antifungal Activity of the Biogenic AgNPs with Commonly Used Antifungal Agents

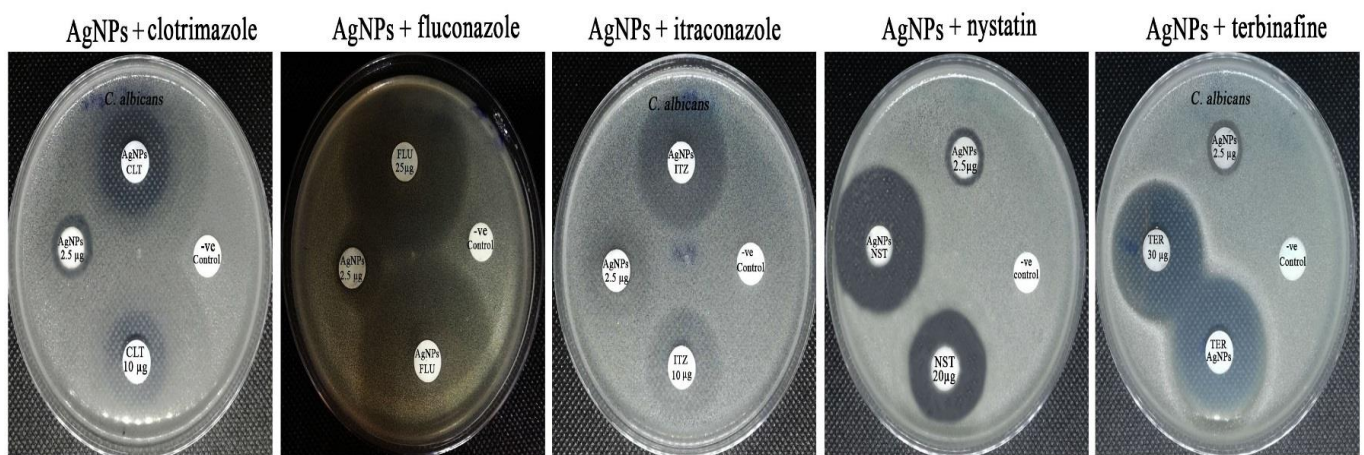
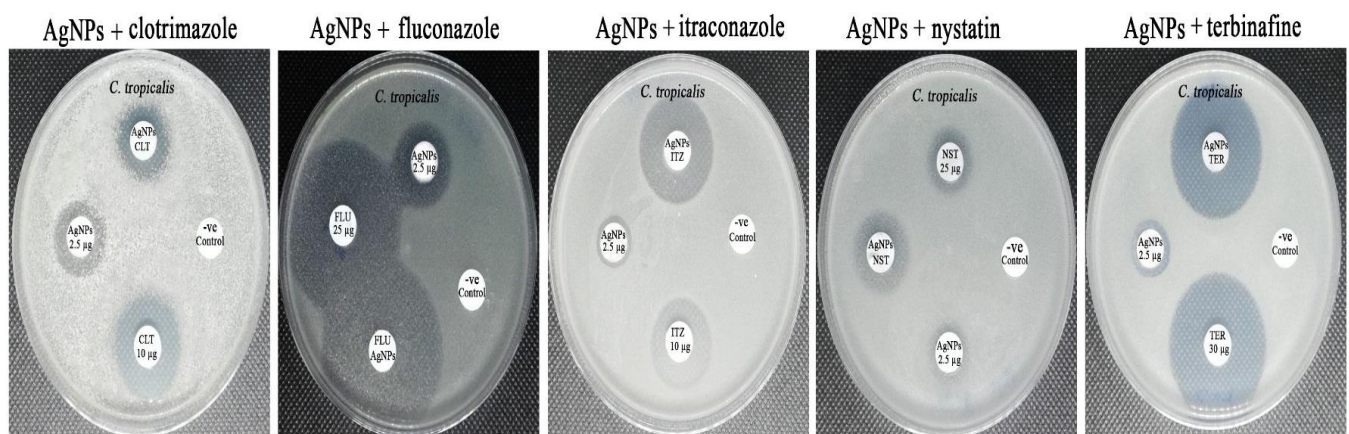
The *Candida glabrata* strain was found to be resistant to terbinafine, nystatin, and itraconazole antifungal drugs. This result was consistent with that of a previous report which investigated the resistance pattern of 22 clinical isolates of *C. glabrata* and reported their resistance to nystatin and itraconazole drugs [66].

The MIC concentration of the biosynthesized AgNPs was investigated for their synergistic efficiency against the concerned candidal strains. A disc diffusion assay was performed to detect the synergistic efficiency of biogenic AgNPs in combination with antifungal agents against the tested 12 candida strains. Silver nanoparticles in combination with itraconazole antifungal agent showed the highest synergistic efficiency against *C. glabrata*, *C. albicans*, and *C. tropicalis*, recording relative synergism percentages of 74.32%, 57.78, and 36.37%, respectively. Antimicrobial assays of AgNPs in combination with antifungal agents clearly confirmed the potent synergistic action of the biogenic AgNPs with itraconazole antifungal agent against *C. albicans*, *C. tropicalis*, and *C. glabrata*, as seen in Figures 10–12, respectively. In addition, terbinafine and nystatin antifungal agents exhibited a high synergistic efficiency against *C. glabrata* and *C. albicans* strains, recording synergism percentages of 59.13 and 42.66%, respectively. Our findings matched those of a previous study, which found that nystatin combined with AgNPs synthesized using *Tagetes erecta* aqueous flower extract revealed synergistic antifungal action against the *C. albicans* strain [67]. Taken together, the biosynthesized AgNPs showed promising synergistic activity with nystatin antifungal agent against multidrug-resistant candidal strains such as *C. glabrata*. In contrast, no interaction was observed between AgNPs and nystatin antifungal agent against the *C. glabrata* strain, while antagonistic interaction was detected between AgNPs and fluconazole antifungal agent against the same strain, as clearly presented in Table 3. Moreover, a slight synergism was detected between AgNPs and fluconazole antifungal drug against *C. albicans* and *C. tropicalis*, recording synergism percentages of 16.51 and 16.31%, respectively, while AgNPs revealed the least synergistic activity against *C. glabrata* recording the relative percentage of 27.71%, as seen in Figure 13. Our results were consistent with that of a previous study which revealed that the aqueous extract of *Anastatica hierochuntica* mediated green biofabrication of biogenic AgNPs with synergistic efficiency with fluconazole antifungal drug [68]. AgNPs were found to have sizes ranging from 1 to 100 nm, indicating their potential utility as antibacterial and cytotoxic agents, as evidenced by their capacity to easily bind to cell walls [69]. This attachment resulted in an adverse impact on cellular permeability and respiration, causing cell death [70]. Furthermore, AgNPs were reported to be able to also certainly enter cells to interact with vital molecules, including protein and DNA, via their sulfur and phosphorus groups, respectively, resulting in disruption of these biomolecules and induction of cell death [71].

Table 3. Antimicrobial activity of biogenic silver nanoparticles in combination with common antifungal agents.

Concentrations ($\mu\text{g}/\text{Disk}$)	Inhibition Zone Diameter (mm)					
	<i>C. albicans</i>	<i>C. glabrata</i>	<i>C. tropicalis</i>	S	I	R
CLO (10 μg)	24.68 \pm 0.34	35.89 \pm 0.32	23.89 \pm 0.45	≥ 20	12–19	<11
CLO (10 μg) + AgNPs (2.5 μg)	24.78 \pm 0.15	27.91 \pm 0.42	17.78 \pm 0.36			
FLU (25 μg)	45.31 \pm 0.12	22.12 \pm 0.17	43.56 \pm 0.41	≥ 22	15–21	<14
FLU (25 μg) + AgNPs (2.5 μg)	34.41 \pm 0.16	19.34 \pm 0.23	37.45 \pm 0.26			
ITZ (10 μg)	38.23 \pm 0.31	8.01 \pm 0.07	20.92 \pm 0.31	≥ 23	14–22	<13
ITZ (10 μg) + AgNPs (2.5 μg)	24.26 \pm 0.25	14.12 \pm 0.36	29.78 \pm 0.20			
NST (25 μg)	32.16 \pm 0.47	0.00 \pm 0.00	15.89 \pm 0.36	≥ 15	10–19	<10
NST (25 μg) + AgNPs (2.5 μg)	42.14 \pm 0.36	0.00 \pm 0.00	22.67 \pm 0.24			
TER (30 μg)	31.76 \pm 0.51	8.21 \pm 0.08	34.98 \pm 0.27	≥ 20	12–19	<11
TER (30 μg) + AgNPs (2.5 μg)	37.98 \pm 0.43	12.89 \pm 0.21	33.76 \pm 0.13			

S: susceptible, I: intermediate, R: resistant.

**Figure 10.** Synergistic pattern of biogenic AgNPs with different antifungal agents against *C. albicans* strain.**Figure 11.** Synergistic patterns of biogenic AgNPs with different antifungal agents against *C. tropicalis* strain.

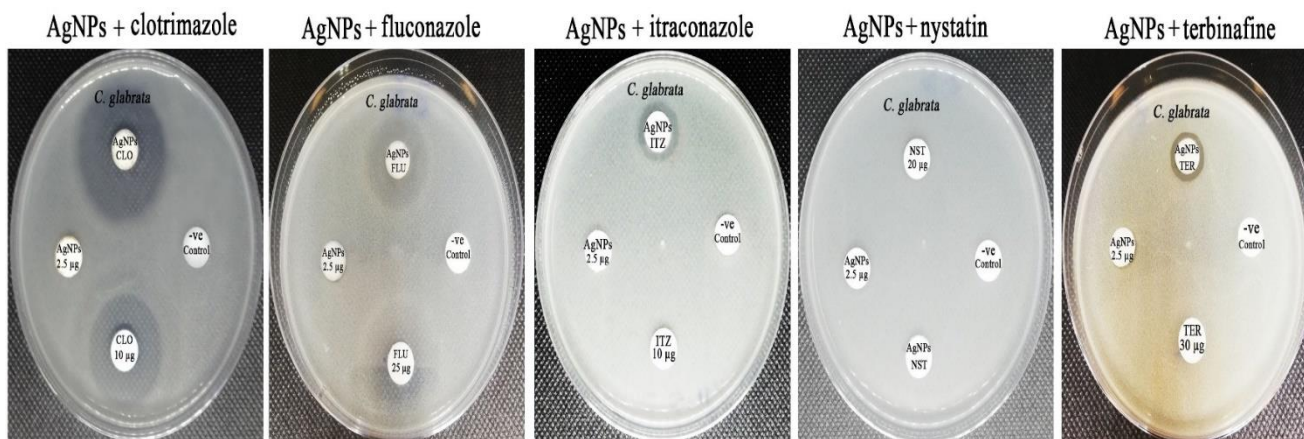


Figure 12. Synergistic patterns of biogenic AgNPs with different antifungal agents against *C. glabrata* strain.

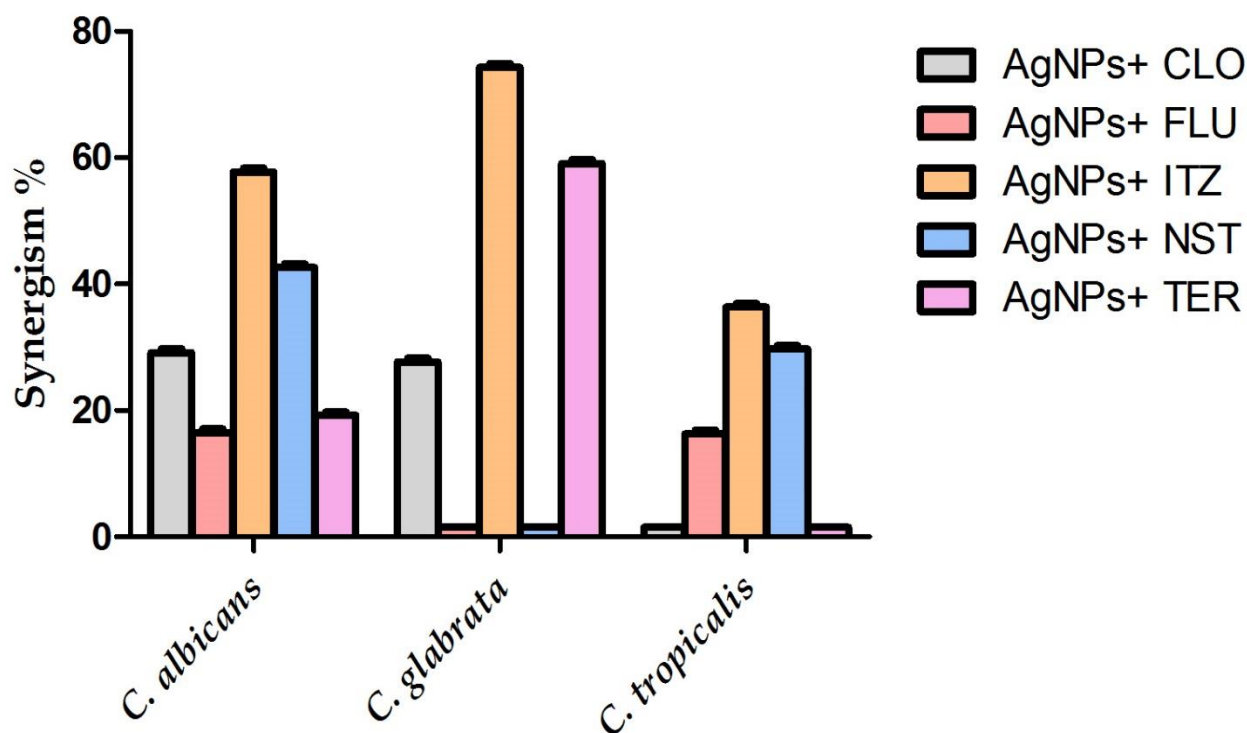


Figure 13. Synergistic percentages (%) of the biogenic silver nanoparticles with common antifungal drugs.

Previous studies demonstrated the synergistic mode of action between AgNPs and antifungal drugs demonstrating that chlorhexidine dingluconate and nystatin could disrupt the candidal cell membranes, resulting in changes in cell permeability and the leakage of cell constituents, whereas AgNPs could bind to sulphur-containing proteins, causing cell membrane disruption, interrelating with phosphorus-containing compounds, and finally disruption of the respiratory chain [28,72]. Another study investigated the synergistic antifungal effectiveness between azole antifungal drugs such as fluconazole or voriconazole and polyvinylpyrrolidone-coated AgNPs, finding that the PVP-coated AgNPs bonded to the cellular membranes and suppressed the budding replication, resulting in synergistic antifungal action with fluconazole or voriconazole in fungal cells [73]. Moreover, the synergistic mode of action was demonstrated by another study between echinocandin drugs as caspofungin or micafungin and chemically synthesized AgNPs, hypothesizing

that echinocandin drugs suppressed the enzymatic action of β -1,3-d-glucan synthase that is necessary for cell wall synthesis causing disruption of fungal cell walls, facilitating the entry of Ag NPs into the fungal cells and disrupting purine metabolism and finally incidence of cell death [74]. Collectively, we hypothesized that both itraconazole drugs and the biogenic AgNPs demonstrated synergistic antifungal mode of action as both itraconazole and AgNPs targeted different fungal cellular constituents. In this regard, itraconazole interferes with the 14- α demethylase enzyme, which is required for the conversion of lanosterol to ergosterol, an important component of the fungal cell membrane, resulting in the inhibition of ergosterol synthesis, increasing the cellular permeability and finally leakage of the fungal cellular constituents [75]. On the other hand, the biogenic AgNPs bind to vital cellular constituents of candidal cells as DNA and protein via phosphorous and sulfur groups resulting in the induction of fungal cell death [76].

4. Conclusions

The biogenic silver nanoparticles exhibited a potential antifungal activity against the tested candidal strains. *Candida tropicalis* was the most sensitive strain to the biogenic AgNPs synthesized using the aqueous peel extract of *P. granatum*. AgNPs showed the highest synergistic efficiency with itraconazole drugs against different fungal pathogens. The potential synergistic efficiency of the biogenic AgNPs with antifungal agents such as itraconazole, terbinafine, and clotrimazole against *C. glabrata* as a multi-drug resistant strain confirmed the potential usage of the biosynthesized silver nanomaterials in combination with these agents in formulation of highly effective antifungal agents against multidrug-resistant strains.

Author Contributions: Conceptualization, M.T.Y. and A.A.A.-A.; methodology, M.T.Y.; software, M.T.Y.; validation, M.T.Y., A.A.A.-A. and F.O.A.-O.; formal analysis, A.A.A.-A., F.O.A.-O. and A.A.-F.M.; investigation, M.T.Y.; resources, A.A.A.-A.; data curation, M.T.Y.; writing—original draft preparation, M.T.Y.; writing—review and editing, A.A.-F.M., A.A.A.-A. and F.O.A.-O.; visualization, A.A.-F.M.; supervision, A.A.A.-A.; project administration, A.A.A.-A.; funding acquisition, A.A.A.-A. All authors have read and agreed to the published version of the manuscript.

Funding: The study was funded by the Researchers Supporting Project number (RSP-2021/362), King Saud University, Riyadh, Saudi Arabia.

Data Availability Statement: The datasets used and/or analyzed during the current study are available from the corresponding author upon reasonable request.

Acknowledgments: The authors extend their appreciation to the Researchers Supporting Project number (RSP-2021/362), King Saud University, Riyadh, Saudi Arabia.

Conflicts of Interest: The authors declare no conflict of interest.

References

1. Rubey, K.M.; Brenner, J.S. Nanomedicine to fight infectious disease. *Adv. Drug Deliv. Rev.* **2021**, *179*, 113996. [[CrossRef](#)] [[PubMed](#)]
2. Bongomin, F.; Gago, S.; Oladele, R.O.; Denning, D.W. Global and multi-national prevalence of fungal diseases—Estimate precision. *J. Fungi* **2017**, *3*, 57. [[CrossRef](#)] [[PubMed](#)]
3. Jorgensen, S.C.; Trinh, T.D.; Zasowski, E.J.; Lagnf, A.M.; Simon, S.P.; Bhatia, S.; Melvin, S.M.; Steed, M.E.; Finch, N.A.; Morrisette, T.; et al. Real-world experience with ceftolozane-tazobactam for multidrug-resistant gram-negative bacterial infections. *Antimicrob. Agents Chemother.* **2020**, *64*, e02291-19. [[CrossRef](#)] [[PubMed](#)]
4. Francesconi, F.; Jalkh, A.P.; Lupi, O.; Khalfe, Y. *Mechanisms of Antifungal Drug Resistance Overcoming Antimicrobial Resistance of the Skin*; Springer: Berlin/Heidelberg, Germany, 2021; pp. 133–142.
5. Ibe, C.; Oladele, R.O.; Alamir, O. Our pursuit for effective antifungal agents targeting fungal cell wall components: Where are we? *Int. J. Antimicrob. Agents* **2021**, *59*, 106477. [[CrossRef](#)]
6. Allen, D.; Wilson, D.; Drew, R.; Perfect, J. Azole antifungals: 35 years of invasive fungal infection management. *Expert Rev. Anti-Infect. Ther.* **2015**, *13*, 787–798. [[CrossRef](#)]
7. Sardari, A.; Zarrinfar, H.; Mohammadi, R. Detection of ERG11 point mutations in Iranian fluconazole-resistant *Candida albicans* isolates. *Curr. Med. Mycol.* **2019**, *5*, 7.
8. Lee, Y.; Puumala, E.; Robbins, N.; Cowen, L.E. Antifungal drug resistance: Molecular mechanisms in *Candida albicans* and beyond. *Chem. Rev.* **2020**, *121*, 3390–3411. [[CrossRef](#)]

9. Bhattacharya, S.; Sae-Tia, S.; Fries, B.C. Candidiasis and mechanisms of antifungal resistance. *Antibiotics* **2020**, *9*, 312. [[CrossRef](#)]
10. Nishimoto, A.T.; Sharma, C.; Rogers, P.D. Molecular and genetic basis of azole antifungal resistance in the opportunistic pathogenic fungus *Candida albicans*. *J. Antimicrob. Chemother.* **2020**, *75*, 257–270. [[CrossRef](#)]
11. Revie, N.M.; Iyer, K.R.; Robbins, N.; Cowen, L.E. Antifungal drug resistance: Evolution, mechanisms and impact. *Curr. Opin. Microbiol.* **2018**, *45*, 70–76. [[CrossRef](#)]
12. Robbins, N.; Cowen, L.E. Antifungal drug resistance: Deciphering the mechanisms governing multidrug resistance in the fungal pathogen *Candida glabrata*. *Curr. Biol.* **2021**, *31*, R1520–R1523. [[CrossRef](#)]
13. Pinto, M.; Borges, V.; Nascimento, M.; Martins, F.; Pessanha, M.A.; Faria, I.; Rodrigues, J.; Matias, R.; Gomes, J.P.; Jordao, L. Insights on catheter-related bloodstream infections: A prospective observational study on the catheter colonization and multidrug resistance. *J. Hosp. Infect.* **2022**, *123*, 43–51. [[CrossRef](#)]
14. Gheorghe, D.C.; Niculescu, A.-G.; Bîrcă, A.C.; Grumezescu, A.M. Biomaterials for the prevention of oral candidiasis development. *Pharmaceutics* **2021**, *13*, 803. [[CrossRef](#)]
15. Dey, N.; Kamatchi, C.; Vickram, A.S.; Anbarasu, K.; Thanigaivel, S.; Palanivelu, J.; Pugazhendhi, A.; Ponnusamy, V.K. Role of nanomaterials in deactivating multiple drug resistance efflux pumps—A review. *Environ. Res.* **2022**, *204*, 111968. [[CrossRef](#)]
16. Behzad, F.; Naghib, S.M.; Tabatabaei, S.N.; Zare, Y.; Rhee, K.Y. An overview of the plant-mediated green synthesis of noble metal nanoparticles for antibacterial applications. *J. Ind. Eng. Chem.* **2021**, *94*, 92–104. [[CrossRef](#)]
17. Carrillo-González, R.; Martínez-Gómez, M.A.; González-Chávez, M.d.C.A.; Hernández, J.C.M. Inhibition of microorganisms involved in deterioration of an archaeological site by silver nanoparticles produced by a green synthesis method. *Sci. Total Environ.* **2016**, *565*, 872–881. [[CrossRef](#)]
18. Yaqoob, A.A.; Umar, K.; Ibrahim, M.N.M. Silver nanoparticles: Various methods of synthesis, size affecting factors and their potential applications—a review. *Appl. Nanosci.* **2020**, *10*, 1369–1378. [[CrossRef](#)]
19. Paul, S.; Mohanram, K.; Kannan, I. Antifungal activity of curcumin-silver nanoparticles against fluconazole-resistant clinical isolates of *Candida* species. *Ayu* **2018**, *39*, 182. [[CrossRef](#)]
20. Iravani, S.; Korbekandi, H.; Mirmohammadi, S.V.; Zolfaghari, B. Synthesis of silver nanoparticles: Chemical, physical and biological methods. *Res. Pharm. Sci.* **2014**, *9*, 385.
21. Hebbalalu, D.; Lalley, J.; Nadagouda, M.N.; Varma, R.S. Greener techniques for the synthesis of silver nanoparticles using plant extracts, enzymes, bacteria, biodegradable polymers, and microwaves. *ACS Sustain. Chem. Eng.* **2013**, *1*, 703–712. [[CrossRef](#)]
22. Jeevanandam, J.; Kiew, S.F.; Boakye-Ansah, S.; Lau, S.Y.; Barhoum, A.; Danquah, M.K.; Rodrigues, J. Green approaches for the synthesis of metal and metal oxide nanoparticles using microbial and plant extracts. *Nanoscale* **2022**, *14*, 2534–2571. [[CrossRef](#)] [[PubMed](#)]
23. Shreyash, N.; Bajpai, S.; Khan, M.A.; Vijay, Y.; Tiwary, S.K.; Sonker, M. Green synthesis of nanoparticles and their biomedical applications: A review. *ACS Appl. Nano Mater.* **2021**, *4*, 11428–11457. [[CrossRef](#)]
24. Kumar, S.; Basumatary, I.B.; Sudhani, H.P.; Bajpai, V.K.; Chen, L.; Shukla, S.; Mukherjee, A. Plant extract mediated silver nanoparticles and their applications as antimicrobials and in sustainable food packaging: A state-of-the-art review. *Trends Food Sci. Technol.* **2021**, *112*, 651–666. [[CrossRef](#)]
25. Perfect, J.R.; Ghannoum, M. Emerging issues in antifungal resistance. *Infect Dis. Clin.* **2020**, *34*, 921–943. [[CrossRef](#)]
26. Sousa, F.; Ferreira, D.; Reis, S.; Costa, P. Current insights on antifungal therapy: Novel nanotechnology approaches for drug delivery systems and new drugs from natural sources. *Pharmaceutics* **2020**, *13*, 248. [[CrossRef](#)]
27. Ijaz, M.; Zafar, M.; Iqbal, T. Green synthesis of silver nanoparticles by using various extracts: A review. *Inorg. Nano Met. Chem.* **2020**, *51*, 744–755. [[CrossRef](#)]
28. Monteiro, D.R.; Silva, S.; Negri, M.; Gorup, L.F.; de Camargo, E.R.; Oliveira, R.; Barbosa, D.B.; Henriques, M. Antifungal activity of silver nanoparticles in combination with nystatin and chlorhexidine digluconate against *Candida albicans* and *Candida glabrata* biofilms. *Mycoses* **2013**, *56*, 672–680. [[CrossRef](#)]
29. Jia, D.; Sun, W. Silver nanoparticles offer a synergistic effect with fluconazole against fluconazole-resistant *Candida albicans* by abrogating drug efflux pumps and increasing endogenous ROS. *Infect. Genet. Evol.* **2021**, *93*, 104937. [[CrossRef](#)]
30. Falcão, C.M.C.; Andrade, A.; Holanda, V.N.; de Figueiredo, R.C.B.Q.; Ximenes, E.A.; Gomes, A.S.L. Activity of poly(methacrylic acid)-silver nanoparticles on fluconazole-resistant *Candida albicans* strains: Synergistic and cytotoxic effects. *J. Appl. Microbiol.* **2022**, *132*, 4300–4309. [[CrossRef](#)]
31. Shi, C.; Liu, J.; Li, W.; Zhao, Y.; Meng, L.; Xiang, M. Expression of fluconazole resistance-associated genes in biofilm from 23 clinical isolates of *Candida albicans*. *Braz. J. Microbiol.* **2019**, *50*, 157–163. [[CrossRef](#)]
32. Yassin, M.T.; Mostafa, A.A.; Al-Askar, A.A.; Bdeer, R. In vitro antifungal resistance profile of *Candida* strains isolated from Saudi women suffering from vulvovaginitis. *Eur. J. Med. Res.* **2020**, *25*, 1. [[CrossRef](#)]
33. Sakagami, T.; Kawano, T.; Yamashita, K.; Yamada, E.; Fujino, N.; Kaeriyama, M.; Fukuda, Y.; Nomura, N.; Mitsuyama, J.; Suematsu, H.; et al. Antifungal susceptibility trend and analysis of resistance mechanism for *Candida* species isolated from bloodstream at a Japanese university hospital. *J. Infect. Chemother.* **2019**, *25*, 34–40. [[CrossRef](#)]
34. Aldardeer, N.F.; Albar, H.; Al-Attas, M.; Eldali, A.; Qutub, M.; Hassanien, A.; Alraddadi, B. Antifungal resistance in patients with *Candidaemia*: A retrospective cohort study. *BMC Infect. Dis.* **2020**, *20*, 55. [[CrossRef](#)]

35. Yassin, M.T.; Mostafa, A.A.F.; Al-Askar, A.A.; Al-Otibi, F.O. Facile Green Synthesis of Silver Nanoparticles Using Aqueous Leaf Extract of *Origanum majorana* with Potential Bioactivity against Multidrug Resistant Bacterial Strains. *Crystals* **2022**, *12*, 603. [[CrossRef](#)]
36. Rao, B.; Tang, R.-C. Green synthesis of silver nanoparticles with antibacterial activities using aqueous *Eriobotrya japonica* leaf extract. *Adv. Nat. Sci. Nanosci. Nanotechnol.* **2017**, *8*, 015014. [[CrossRef](#)]
37. Khan, M.; Karuppiah, P.; Alkhatlan, H.Z.; Kuniyil, M.; Khan, M.; Adil, S.F.; Shaik, M.R. Green Synthesis of Silver Nanoparticles Using *Juniperus procera* Extract: Their Characterization, and Biological Activity. *Crystals* **2022**, *12*, 420. [[CrossRef](#)]
38. Ahmed, F.; AlOmar, S.Y.; Albalawi, F.; Arshi, N.; Dwivedi, S.; Kumar, S.; Shaalan, N.M.; Ahmad, N. Microwave Mediated Fast Synthesis of Silver Nanoparticles and Investigation of Their Antibacterial Activities for Gram-Positive and Gram-Negative Microorganisms. *Crystals* **2021**, *11*, 666. [[CrossRef](#)]
39. Yi, Y.; Wang, C.; Cheng, X.; Yi, K.; Huang, W.; Yu, H. Biosynthesis of Silver Nanoparticles by *Conyza canadensis* and Their Antifungal Activity against *Bipolaris maydis*. *Crystals* **2021**, *11*, 1443. [[CrossRef](#)]
40. CLSI. *Method for Antifungal Disk Diffusion Susceptibility Testing of Yeasts*; CLSI m44-a; Clinical and Laboratory Standards Institute: Wayne, PA, USA, 2004; Volume 23.
41. CLSI. *Performance Standards for Antifungal Susceptibility Testing of Yeasts*, CLSI Supplement m60, 1st ed.; Clinical and Laboratory Standards Institute: Wayne, PA, USA, 2017.
42. Yassin, M.T.; Mostafa, A.A.F.; Al Askar, A.A. In Vitro Evaluation of Biological Activities and Phytochemical Analysis of Different Solvent Extracts of *Punica granatum* L. (Pomegranate) Peels. *Plants* **2021**, *10*, 2742. [[CrossRef](#)]
43. Singh, R.; Wagh, P.; Wadhvani, S.; Gaidhani, S.; Kumbhar, A.; Bellare, J.; Chopade, B.A. Synthesis, optimization, and characterization of silver nanoparticles from *Acinetobacter calcoaceticus* and their enhanced antibacterial activity when combined with antibiotics. *Int. J. Nanomed.* **2013**, *8*, 4277.
44. Huang, W.; Yan, M.; Duan, H.; Bi, Y.; Cheng, X.; Yu, H. Synergistic antifungal activity of green synthesized silver nanoparticles and epoxiconazole against *Setosphaeria turcica*. *J. Nanomater.* **2020**, *2020*, 9535432. [[CrossRef](#)]
45. Lo, W.H.; Deng, F.S.; Chang, C.J.; Lin, C.H. Synergistic antifungal activity of chitosan with fluconazole against *Candida albicans*, *Candida tropicalis*, and fluconazole-resistant strains. *Molecules* **2020**, *25*, 5114. [[CrossRef](#)] [[PubMed](#)]
46. Moteriya, P.; Padalia, H.; Chanda, S. Characterization, synergistic antibacterial and free radical scavenging efficacy of silver nanoparticles synthesized using *Cassia roxburghii* leaf extract. *J. Genet. Eng. Biotechnol.* **2017**, *15*, 505–513. [[CrossRef](#)] [[PubMed](#)]
47. Zia, M.; Gul, S.; Akhtar, J.; Ul Haq, I.; Abbasi, B.H.; Hussain, A.; Naz, S.; Chaudhary, M.F. Green synthesis of silver nanoparticles from grape and tomato juices and evaluation of biological activities. *IET Nanobiotechnol.* **2017**, *11*, 193–199. [[CrossRef](#)]
48. Bélteky, P.; Rónavári, A.; Zakupszky, D.; Boka, E.; Igaz, N.; Szerencsés, B.; Pfeiffer, I.; Vágvölgyi, C.; Kiricsi, M.; Kónya, Z. Are smaller nanoparticles always better? Understanding the biological effect of size-dependent silver nanoparticle aggregation under biorelevant conditions. *Int. J. Nanomed.* **2021**, *16*, 3021. [[CrossRef](#)]
49. Shehabeldine, A.M.; Elbahnasawy, M.A.; Hasaballah, A.I. Green phytosynthesis of silver nanoparticles using *Echinochloa stagnina* extract with reference to their antibacterial, cytotoxic, and larvicidal activities. *BioNanoScience* **2021**, *11*, 526–538. [[CrossRef](#)]
50. Vallinayagam, S.; Rajendran, K.; Sekar, V. Green synthesis and characterization of silver nanoparticles using *Naringi crenulate* leaf extract: Key challenges for anticancer activities. *J. Mol. Struct.* **2021**, *1243*, 130829. [[CrossRef](#)]
51. Mortazavi-Derazkola, S.; Ebrahimzadeh, M.A.; Amiri, O.; Goli, H.R.; Rafiei, A.; Kardan, M.; Salavati-Niasari, M. Facile green synthesis and characterization of *Crataegus microphylla* extract-capped silver nanoparticles (CME@ Ag-NPs) and its potential antibacterial and anticancer activities against AGS and MCF-7 human cancer cells. *J. Alloys Compd.* **2020**, *820*, 153186. [[CrossRef](#)]
52. Restrepo, C.V.; Villa, C.C. Synthesis of silver nanoparticles, influence of capping agents, and dependence on size and shape: A review. *Environ. Nanotechnol. Monit. Manag.* **2021**, *15*, 100428. [[CrossRef](#)]
53. Abdel-Raouf, N.; Al-Enazi, N.M.; Ibraheem, I.B.M.; Alharbi, R.M.; Alkhulaifi, M.M. Biosynthesis of silver nanoparticles by using of the marine brown alga *Padina pavonia* and their characterization. *Saudi J. Biol. Sci.* **2019**, *26*, 1207–1215. [[CrossRef](#)]
54. Dada, A.O.; Adekola, F.A.; Dada, F.E.; Adelani-Akande, A.T.; Bello, M.O.; Okonkwo, C.R.; Inyinbor, A.A.; Oluyori, A.P.; Olayanju, A.; Ajanaku, K.O.; et al. Silver nanoparticle synthesis by *Acalypha wilkesiana* extract: Phytochemical screening, characterization, influence of operational parameters, and preliminary antibacterial testing. *Heliyon* **2019**, *5*, e02517. [[CrossRef](#)]
55. Sila, M.J.; Nyambura, M.I.; Abong'o, D.A.; Mwaura, F.B.; Iwuoha, E. Biosynthesis of silver nanoparticles from *Eucalyptus corymbia* leaf extract at optimized conditions. In *Nano Hybrids and Composites*; Trans Tech Publications Ltd.: Zurich, Switzerland, 2019.
56. Femi-Adepoju, A.G.; Dada, A.O.; Otun, K.O.; Adepoju, A.O.; Fatoba, O.P. Green synthesis of silver nanoparticles using terrestrial fern (*Gleichenia pectinata* (Willd.) C. Presl.): Characterization and antimicrobial studies. *Heliyon* **2019**, *5*, e01543. [[CrossRef](#)]
57. Al Aboody, M.S. Silver/silver chloride (Ag/AgCl) nanoparticles synthesized from *Azadirachta indica* latex and its antibiofilm activity against fluconazole resistant *Candida tropicalis*. *Artif. Cells Nanomed. Biotechnol.* **2019**, *47*, 2107–2113. [[CrossRef](#)]
58. Devanesan, S.; AlSalhi, M.S.; Balaji, R.V.; Ranjitsingh, A.J.A.; Ahamed, A.; Alfuraydi, A.A.; AlQahtani, F.Y.; Aleanizy, F.S.; Othman, A.H. Antimicrobial and cytotoxicity effects of synthesized silver nanoparticles from *Punica granatum* peel extract. *Nanoscale Res. Lett.* **2018**, *13*, 315. [[CrossRef](#)]
59. Soliman, A.M.; Abdel-Latif, W.; Shehata, I.H.; Fouda, A.; Abdo, A.M.; Ahmed, Y.M. Green approach to overcome the resistance pattern of *Candida* spp. using biosynthesized silver nanoparticles fabricated by *Penicillium chrysogenum* F9. *Biol. Trace Elem. Res.* **2021**, *199*, 800–811. [[CrossRef](#)]

60. Estevez, M.B.; Casaux, M.L.; Fraga, M.; Faccio, R.; Alborés, S. Biogenic silver nanoparticles as a strategy in the fight against multi-resistant salmonella enterica isolated from dairy calves. *Front. Bioeng. Biotechnol.* **2021**, *9*, 314. [[CrossRef](#)]
61. Salleh, M.S.N.; Ali, R.R.; Shameli, K.; Hamzah, M.Y.; Kasmani, R.M.; Nasef, M.M. Interaction Insight of Pullulan-Mediated Gamma-Irradiated Silver Nanoparticle Synthesis and Its Antibacterial Activity. *Polymers* **2021**, *13*, 3578. [[CrossRef](#)]
62. Hawar, S.N.; Al-Shmgani, H.S.; Al-Kubaisi, Z.A.; Sulaiman, G.M.; Dewir, Y.H.; Rikisahedew, J.J. Green Synthesis of Silver Nanoparticles from *Alhagi graecorum* Leaf Extract and Evaluation of Their Cytotoxicity and Antifungal Activity. *J. Nanomater.* **2022**, *2022*, 1058119. [[CrossRef](#)]
63. Endo, E.H.; Cortez, D.A.G.; Ueda-Nakamura, T.; Nakamura, C.V.; Dias Filho, B.P. Potent antifungal activity of extracts and pure compound isolated from pomegranate peels and synergism with fluconazole against *Candida albicans*. *Res. Microbiol.* **2010**, *161*, 534–540. [[CrossRef](#)]
64. Ali, S.; Sulaiman, S.; Khan, A.; Khan, M.R.; Khan, R. Green synthesized silver nanoparticles (AgNPs) from *Parrotiopsis jacquemontiana* (Decne) Rehder leaf extract and its biological activities. *Microsc. Res. Tech.* **2022**, *85*, 28–43. [[CrossRef](#)]
65. Sharifi-Rad, M.; Pohl, P. Synthesis of biogenic silver nanoparticles (Agcl-NPs) using a pulicaria vulgaris gaertn. aerial part extract and their application as antibacterial, antifungal and antioxidant agents. *Nanomaterials* **2020**, *10*, 638. [[CrossRef](#)] [[PubMed](#)]
66. Pote, S.T.; Sonawane, M.S.; Rahi, P.; Shah, S.R.; Shouche, Y.S.; Patole, M.S.; Thakar, M.R.; Sharma, R. Distribution of pathogenic yeasts in different clinical samples: Their identification, antifungal susceptibility pattern, and cell invasion assays. *Infect Drug Resist.* **2020**, *13*, 1133. [[CrossRef](#)]
67. Padalia, H.; Moteriya, P.; Chanda, S. Green synthesis of silver nanoparticles from marigold flower and its synergistic antimicrobial potential. *Arab. J. Chem.* **2015**, *8*, 732–741. [[CrossRef](#)]
68. Aabed, K.; Mohammed, A.E. Synergistic and Antagonistic Effects of Biogenic Silver Nanoparticles in Combination With Antibiotics Against Some Pathogenic Microbes. *Front. Bioeng. Biotechnol.* **2021**, *9*, 249. [[CrossRef](#)]
69. Rudramurthy, G.R.; Swamy, M.K. Potential applications of engineered nanoparticles in medicine and biology: An update. *J. Biol. Inorg. Chem.* **2018**, *23*, 1185–1204. [[CrossRef](#)]
70. Tang, S.; Zheng, J. Antibacterial activity of silver nanoparticles: Structural effects. *Adv. Healthc. Mater.* **2018**, *7*, 1701503. [[CrossRef](#)]
71. Cai, X.; Liu, X.; Jiang, J.; Gao, M.; Wang, W.; Zheng, H.; Xu, S.; Li, R. Molecular mechanisms, characterization methods, and utilities of nanoparticle biotransformation in nanosafety assessments. *Small* **2020**, *16*, 1907663. [[CrossRef](#)]
72. Dar, M.A.; Ingle, A.; Rai, M. Enhanced antimicrobial activity of silver nanoparticles synthesized by *Cryphonectria* sp. evaluated singly and in combination with antibiotics. *Nanomed. Nanotechnol. Biol. Med.* **2013**, *9*, 105–110. [[CrossRef](#)]
73. Sun, L.; Liao, K.; Li, Y.; Zhao, L.; Liang, S.; Guo, D.; Hu, J.; Wang, D. Synergy between polyvinylpyrrolidone-coated silver nanoparticles and azole antifungal against drug-resistant *Candida albicans*. *J. Nanosci. Nanotechnol.* **2016**, *16*, 2325–2335. [[CrossRef](#)]
74. Li, H.; Wang, L.; Chai, Y.; Cao, Y.; Lu, F. Synergistic effect between silver nanoparticles and antifungal agents on *Candida albicans* revealed by dynamic surface-enhanced Raman spectroscopy. *Nanotoxicology* **2018**, *12*, 1230–1240. [[CrossRef](#)]
75. Ivanov, M.; Ćirić, A.; Stojković, D. Emerging Antifungal Targets and Strategies. *Int. J. Mol. Sci.* **2022**, *23*, 2756. [[CrossRef](#)] [[PubMed](#)]
76. Nisar, P.; Ali, N.; Rahman, L.; Ali, M.; Shinwari, Z.K. Antimicrobial activities of biologically synthesized metal nanoparticles: An insight into the mechanism of action. *JBIC J. Biol. Inorg. Chem.* **2019**, *24*, 929–941. [[CrossRef](#)] [[PubMed](#)]